HAL
open science

# Low-albedo asteroids: analogues with a high polarization at large phase angles

Edith Hadamcik, Jean-Baptiste Renard, Jérémie Lasue, Anny Chantal Levasseur-Regourd, Masateru Ishiguro

## To cite this version:

Edith Hadamcik, Jean-Baptiste Renard, Jérémie Lasue, Anny Chantal Levasseur-Regourd, Masateru Ishiguro. Low-albedo asteroids: analogues with a high polarization at large phase angles. Monthly Notices of the Royal Astronomical Society, 2022, (in press). 10.1093/mnras/stac2749 . insu-03792625v1

**HAL Id: insu-03792625**

**https://insu.hal.science/insu-03792625v1**

Submitted on 30 Sep 2022 (v1), last revised 9 Feb 2023 (v2)

**HAL** is a multi-disciplinary open access archive for the deposit and dissemination of scientific research documents, whether they are published or not. The documents may come from teaching and research institutions in France or abroad, or from public or private research centers.

L'archive ouverte pluridisciplinaire **HAL**, est destinée au dépôt et à la diffusion de documents scientifiques de niveau recherche, publiés ou non, émanant des établissements d'enseignement et de recherche français ou étrangers, des laboratoires publics ou privés.

# Low-albedo asteroids: analogues with a high polarization at large phase angles

E. Hadamcik[1*], J.-B. Renard[2], J. Lasue[3], A.C. Levasseur-Regourd[†], M. Ishiguro[4,5]

[1]LATMOS-IPSL, CNRS/INSU, 11 bld d'Alembert, F-78280 Guyancourt , France
[2]LPC2E-CNRS, Université d'Orléans, 3A avenue de la recherche scientifique, F-45071 Orléans cedex 2, France
[3]Université Paul Sabatier UPS; IRAP-CNRS, CNES, 9 avenue du Colonel Roche, F-31500, Toulouse, France
[4]Department of Physics and Astronomy, Seoul National University, I Gwanak-ro, Gwanak-gu, Seoul 08826, Republic of Korea
[5]SNU Astronomy Research Center, Seoul National University, , I Gwanak-ro, Gwanak-gu, Seoul 08826, Republic of Korea

**ABSTRACT**

While remote observations of the linear polarization of five low-albedo Near-Earth asteroids are available at large phase angles, space missions have collected material on the surface of two of them and one of them is already back to Earth. The structure of the regolith on the surface may be different from that encountered on larger objects, because of their low gravity and thermal stress cycling. Dust particles crushed from low albedo meteorites (i.e. Orgueil and Allende) are tentatively used as analogues to try and provide a better approach of such regoliths. The PROGRA2 experiment studies the light scattering properties of dust particles of various size distribution*s* under Earth gravity either deposited or with clouds lifted by an air-draught, as well as under μ-gravity conditions. Similar maximum in polarization (i.e., $P_{max}$) values are obtained experimentally for dark particles deposited or in levitation, showing that multiple scattering is negligible. The increased sensitivity of PROGRA2 instruments, together with imaging techniques, make it possible to study $P_{max}$ with increasing sizes of the lifted particles, up to mm-sizes and above. Our results confirm that particles constituting the regolith present mm-size ranges and may reach polarization values up to 50 % in good agreement with remote observations. Some materials are also suggested to be present on the surface of the particles. Also, huge agglomerates made by random ballistic deposition may be considered as relevant analogues e.g. for pebbles and boulders.

**Key words:**
methods:laboratory:solid state -- techniques:Polarimetry –
minor planets,asteroids:general— meteorites, meteors, meteroids

Emails: [1] hadamcik@latmos.ipsl.fr ; [2] jbrenard@cnrs-orleans.fr

[†]A.C. Levasseur-Regourd passed away on August 1st, 2022

## 1 INTRODUCTION

### 1.1 Context of space missions to low-albedo asteroids

The JAXA Hayabusa space missions have been developed to explore near-Earth asteroids (so-called NEAs) and collect samples thereof. The first Hayabusa spacecraft had collected and returned to Earth in 2010 more than 1000 dust particles with sizes below 100 μm from (25143) Itokawa, a S-type NEA (Fujiwara et al., 2006; Yoshikawa et al. 2010). Since then, new missions have been or will be launched to flyby C-type asteroids, deposit instruments, and collect dust particles. C-type asteroids actually form the majority of the small bodies in the outer main belt and usually present low geometric albedos, ranging from 0.03 to 0.1. JAXA Hayabusa2 mission (Watanabe et al. 2017) delivered to Earth in 2020 about 5.4 g of samples collected on the surface and subsurface of asteroid (162173) Ryugu.
NASA OSIRIS-REx mission (Lauretta et al. 2015, 2019) should deliver to Earth in 2023 more than 50 g of samples from asteroid (101955) Bennu.
Images of both Ryugu and Bennu show a few craters and huge fractured boulders with high porosities. The top-like shape of both asteroids is typical of a rubble-pile origin, with evolution under the YORP effect (Barnouin et al. 2019; Walsh et al. 2019; Sakatani et al. 2021).
Finally, the JAXA DESTINY$^+$ spacecraft (Arai et al. 2018; Kruger et al. 2019) is an elaborate technology demonstrator, planned to be launched in 2024 and study by 2028 the dust on the surface and/or ejected by active asteroid (3200) Phaethon, as well as asteroid (155140) 2005 UD, interplanetary, and interstellar dust. Phaethon, the likely parent body of Geminids meteor showers, presents a dust trail (Battams et al. 2020) and is somehow a transition object between comets and asteroids (Licandro et al. 2007). Since it has a low perihelion distance, about 0.14 au, it could indeed be an extinct cometary nucleus that has suffered drastic dehydration stresses (Jewitt 2012). To prepare the mission, this NEA was intensively observed at its close approach to Earth (distance of about 0.017 au on 16 December 2017).
Low-albedo NEAs can indeed be observed polarimetrically over large phase angles whenever close to the Earth, then providing constraints on their properties.

### 1.2 Remote polarimetric observations of light scattered by low-albedo NEAs

The polarization of the light scattered by surfaces of low-albedo (<0.1) NEAs has been observed remotely at large phase angles, allowing the retrieval of their polarization phase curves (PPC) up to the region where their polarization reaches its maximum ($P_{max}$), for a phase angle ($\alpha_{max}$). Fig 1 presents in the red wavelength domain, the PPC of the five asteroids considered in this paper and shows their high polarization at large phase angles, while Table 1 summarizes their main characteristics. The other parameters of the PPC may also be deduced e.g. phase angle at inversion $\alpha_0$, slope at inversion h, extreme amplitude of the polarization on the negative branch $P_{min}$.

(i) The PPCs for Ryugu and 1998 KU2 are close to one another (Kuroda et al. 2018; Kuroda et al 2021). The $P_{max}$ for Ryugu is estimated to be equal to (54.5 ± 0.5) % for $\alpha_{max}$ = (104 ± 5)°. For 1998 KU2, $P_{max}$ is about (52 ± 5) % for $\alpha_{max}$ = (100 ± 10)°, where the larger error bar is due to the limited number of data points.
(ii) The data for Bennu were obtained by Cellino et al. (2018) up to a phase angle of 57°, they compared its polarimetric phase curve to those F-type and B-type asteroids. Cellino et al., (2019) suggested an F-type asteroid and a higher polarization at large phase angles than for Phaethon i.e. $P_{max}$> 43 % (Table 1). The number of data is too small in a phase angle range limited to 57° to allow a reasonable extrapolation up to $P_{max}$. Interestingly enough the PPC of Bennu is quite similar to that of comet Hale-Bopp (Cellino et al. 2018). for which $P_{max}$ = (32.5 ± 5) % at $\alpha_{max}$ = (90 ± 5)°, with a trigonometric fit (the number of data points allowing the extrapolation with a reasonable confidence level. These values were also found with a numerical model by Zubko et al. (2016).
(iii) Phaethon data correspond to 5 sets obtained in red and visible domains, at different epochs (lower curve data from observations on 27 November to 24 January 2022 (Devogèle et al. 2018; Shinnaka et al. 2018; Kiselev et al., 2022; Geem al., 2022). Above and with a common region up to 30° with the previous curve, data from observations in the red domain obtained in September-October 2016 can be noticed (Ito et al, 2018), as well as two data points obtained in December 16-17 2017 without any filter, which are noted '2017z' (Zheltobryukhov et al. 2018). The PPC for 2005 UD is close to the polarization obtained for Phaethon in 1996 (Devogèle et al. 2020; Ishiguro et al. 2021).

In the present work, experimental studies conducted in laboratory with different types of deposited and levitating particles are used to interpret the high polarization values measured for these very low surface albedo asteroids.

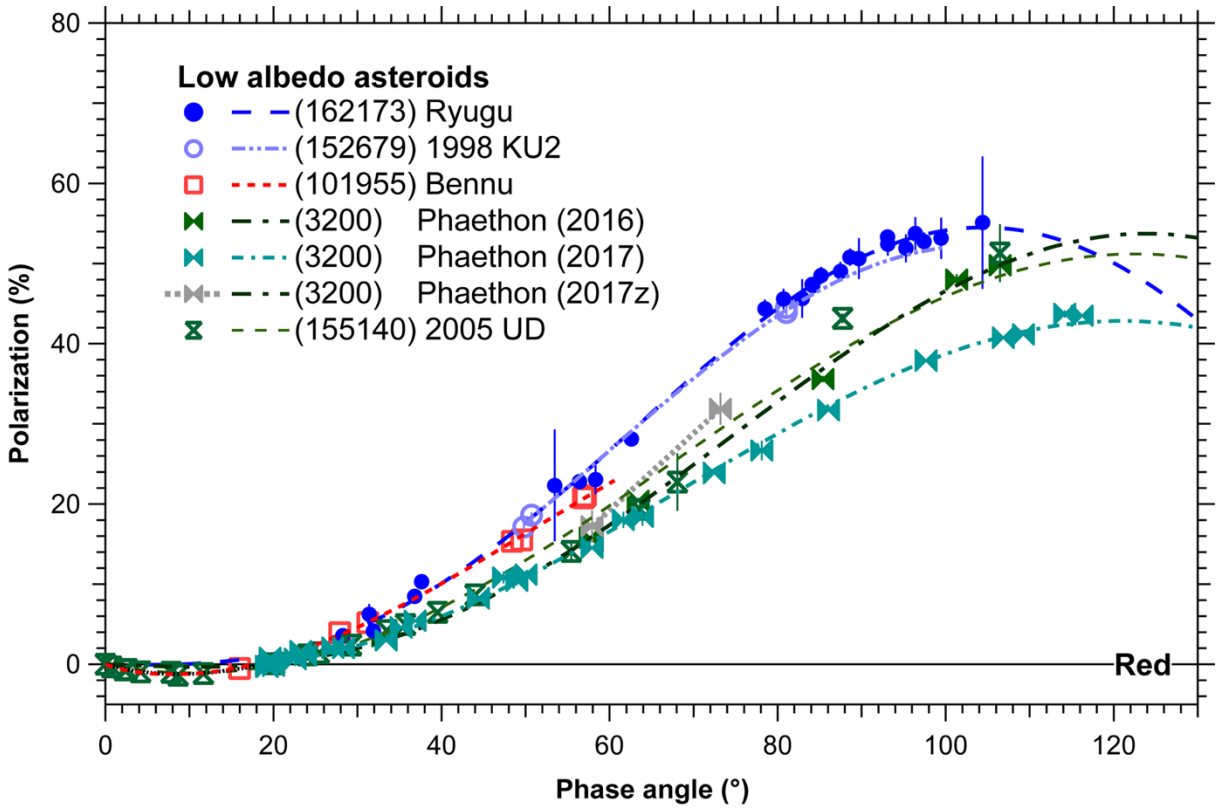


**Figure 1.** PPCs of low-albedo Near Earth Asteroids in the red wavelength domain (except for Phaethon 2017z). Series of values on the same night were averaged for clarity.

### 1.3 Polarization phase curves

To relate the observables (polarization, albedo) to some physical properties of minerals and carbonaceous particles (size-distribution, porosities, surface roughness), results from previous observations of some Solar System bodies and from experimental studies are presented for optically absorbing samples.

The light scattered by the surface of an object without atmosphere, covered by dust particles (e.g. the Moon or asteroids) is partially linearly polarized. The polarization depends on the geometry of observations (phase angle $\alpha$). The polarization value $P_r$ is derived from equation 1

$$P_r = \frac{(I_\perp - I_\parallel)}{(I_\perp + I_\parallel)} \qquad (1)$$

where $I_\perp$ and $I_\parallel$ are the scattered light intensities perpendicular and parallel to the scattering plane, the total intensity being $(I_\perp + I_\parallel)$.

**Table 1.** Characteristics of low albedo NEAs for which polarimetric measurements are available. References for the different characteristics: [1]Sugita et al. 2019; [2]Watanabe et al. 2019; [3]JPL Small Body Data; [4]Nugent et al. 2016; [5]Lauretta et al. 2019; [6]Chesley et al. 2014; [7]Cellino et al. 2018; [8]Hanus et al. 2016; [9]Masiero et al. 2019.

| | Origin of polarimetric data | Main characteristics and parameters |
|---|---|---|
| (162173) Ryugu | Kuroda et al. 2021 | C-type (Apollo)<br>Sample returned by Hayabusa2 in 2020<br>[1]Albedo 0.045 ± 0.002 (at 550 nm)<br>[2]D (equatorial) = 1,004 km<br>[2]Bulk density 1190 ± 20 kg. $m^{-3}$ (porosity 50 %)<br>[2]Perihelion 0.96 au<br>[2]Rubble pile<br>Phase angle range 28° < $\alpha$ < 104°<br>At $\alpha$ = 104°, $P_r$ = 55 % |
| (152679) 1998 KU2 | Kuroda et al. 2018 | C-type (Apollo)<br>(or Ch/(Cgh)-type from SMASS)<br>Albedo [3]0.022/[4]0.03 (NEOWISE)<br>[3]D = 4.167 km<br>[3]Perihelion 1.01 au<br>Phase angle range 50° < $\alpha$ < 81°<br>At 81°, $P_r$ =44.6 %<br>$P_{max}$= (48.8 ± 5.2) % (estimated) |
| (101955) Bennu | Cellino et al. 2018 | [5]B-type (Apollo), B/F-type by Polarimetry<br>Active asteroid<br>Sample return expected by OSIRIS--REx in 2023<br>[5]Albedo 0.044 ± 0.002<br>[5]D ≈ 0.490 km<br>[6]Perihelion 0.90 au<br>[5]Bulk density 1190 ± 13 kg.$m^{-3}$<br>[5]Macroporosity 50 %<br>[5]Rubble pile<br>Phase angle range 16°< $\alpha$ < 57°<br>[7]$\alpha_0$ =17.88°± 0.40; h=0.276 ± 0.012 %/°<br>At [7]$\alpha$ = 57°, $P_r$ = 21% ([7]similar PPC than comet Hale-Bopp) |
| (3200) Phaethon | [f]Fornasier et al., 2006<br>[i]Ito et al. 2018;<br>[s]Shinnaka et al. 2018;<br>[b]Borisov et al. 2018;<br>[d]Devogèle et al. 2018;<br>[z]Zheltobryukhov et al. 2018;<br>[o]Okasaki et al. 2020<br>[k]Kiselev et al., 2022<br>[g]Geem et al., 2022 | B or F-type (Apollo)<br>Active object, quite possibly of cometary origin<br>Origin of the Geminids meteor stream<br>Flyby by DESTINY$^+$ in 2028<br>Albedo[8] 0.12 ± 0.008 (visible)<br>[9] 0.16 ± 0.02 NEOWISE<br>[7]D 5.1 ± 0.2 km<br>[8]Perihelion 0.14 au<br>Phase angle ranges 33° < $\alpha$ < 106.5° for [i] 2016<br>8.8° < $\alpha$ < 134.9° for [s,d,o,k,g,f] 2017-2022<br>$\alpha_0$ = 19.9° ± 0.5° for 2017-2022 observations, V filter<br>h = 0.22 ± 0.05 %/° (this work), V filter<br>[i] $P_r$ =50 % for 2016, at $\alpha$ = 106.5°<br>[d] $P_r$ =44.5 % for 2017, at $\alpha$ = 116.3° |
| (155140) 2005 UD | [d]Devogèle et al. 2020<br>[i]Ishiguro et al. 2021 | B or F-type (Similar to Phaethon)<br>Flyby by DESTINY$^+$ (extended)<br>[9]Albedo 0.14 ± 0.09 (NEOWISE)<br>[i] 0.088-0.109 (polarization in visible)<br>[9]D = 1.2 ± 0.4 km; [i] D= 1.32 ±0.06 km<br>Perihelion 0.16 au<br>Phase angle range 0.74° < $\alpha$ < 106.5°<br>[I] $\alpha_0$= 19.71° ± 0.14°<br>[i]h = 0.197 ± 0.004 %/°<br>At $\alpha$ = 106.5°, $P_r$ = 51 ± 4 % |

### 1.3.1 Umov effect

The brighter the powder, the lower its linear polarization (Umov 1905), is the expression of the so-called Umov effect. This effect shows an inverse correlation between the polarization values and the albedo (proportional to the total intensity). The geometric albedo (A) of any planetary body illuminated by the Sun is the ratio of its brightness observed at opposition to that of an idealized flat Lambertian disc having the same cross-section. The relation is particularly accurate near the maximum polarization ($P_{max}$). A linear dependence can be written in log-log scale:

$\log (P_{max}) + a \log (A) = b$ (2)

where a and b are coefficients dependent on the physical properties of the sample.

When the measurements of the geometric albedo are impossible at opposition, observations for phase angles as small as possible are considered (e.g. 5°-6° or 8°).

Numerous remote observations of particulate surfaces for e.g. the Moon or layers of solid particles in experiments agree with Umov' effect (e.g. Dollfus & Bowell 1971; Dollfus, Bowell & Titulaer, 1971; Shkuratov & Opanasenko 1992; Hadamcik et al. 2002). If the difference $(I_{\perp} - I_{\parallel})$ does not depend on albedo, there is an inverse correlation between log ($P_{max}$) and log (A) and the coefficients can be determined for each kind of samples (Dollfus & Bowell 1971; Zubko et al. 2011). More generally, the parameter (b) depends upon the size and porosity of the particulates and the roughness of the surface layer (Levasseur-Regourd, Hadamcik & Lasue 2006; Shkuratov et al. 2011). The Umov effect appears to be induced by multiple scattering between the particles (or between the constituent grains within their aggregates), which increases the albedo and therefore decreases the polarization (Zubko et al. 2011). The Umov law was also verified for mixtures of high porosity aggregates with silica constituent grains (transparent material) and carbon black (very absorbing material) (Hadamcik et al. 2006).

The phase angle $\alpha_{max,}$ increases when $P_{max}$ increases for observations of different lunar regions (Dollfus & Bowell 1971). In general, it is also the case for powedered artificial glasses having different absorptions (Shkuratov & Opanasenko 1992). For transparent particles in the same size range, the shift in $\alpha_{max}$ is higher than for absorbing ones and increases when the size of the particles increases (Levasseur-Regourd et al. 2015).

Results obtained for layers and for lifted particles in optically thin clouds (single scattering between the particles) are compared. For samples with albedo greater than 0.1 (semi-transparent materials), $P_{max}$ is smaller for layers as compared to lifted particles due to multiple scattering between the particles (Shkuratov et al. 2006; 2007). When the material is darker, as is the case of the Pinatubo volcanic ash observed in blue light with an albedo 0.08 (Shkuratov et al. 2006), $P_{max}$ not being available, the slope h may be used for the comparison. It is very similar for deposited and lifted particles (single scattering). When $P_{max}$ is not accessible, as for main belt asteroids that have a phase angle range limited to about 30°, it is possible to use the slope h at inversion and/or $P_{min}$. The relation (2) may be written:

$\log A = a \log h + b$ (3)

The use of this relation is limited for very dark surfaces, with a saturation of the slope for albedos below 0.06 (Geake & Dollfus 1986). Cellino et al. (2015) have suggested, to determine the geometric albedo of asteroids from empirical relationships between PPC parameters such as the one between the Umov law and the slope h. Coefficients, together with their uncertainties, need to be accurately calibrated

The most common group amongst low-albedo asteroids is the C-group for carbonaceous type. The different sub-classes and their average properties may be found in Belskaya et al. (2017).

### 1.3.2 Experimental PPC obtained with very dark materials

The word 'grains' is used for constituent grains in fluffy aggregates and in solid (compact) and porous particles, following the definitions given by Güttler et al. (2019).

Light scattering by materials mainly made of carbon are usually dark and can be studied in laboratory for different structures and sizes. Muñoz et al. (2020) have studied up to mm-sized particles of various compositions and porosities: (i) a highly absorbing mm-sized charcoal particle presents a $P_{max} \approx 80\%$ in average at $\alpha_{max} \approx 115°$; (ii) two μm-sized particles with nm-sized constituent grains with respectively a $P_{max}$ of 57 % and 86 % at $\alpha_{max} \approx 90°$ (without indication of their composition), are close to the Rayleigh regime. Previously such fluffy particles made of nm-sized constituent grains were studied in μm- to

mm-sized aggregates, made of different transparent or absorbing materials (Volten et al. 2007; Hadamcik et al. 2007a). In the Rayleigh regime, their $P_{max}$ is higher than 40 % increasing with decreasing size of the grains and increasing porosity of the particles.

More specifically, the PROGRA2 experiment was dedicated to the study of light scattered by solid particles deposited on a surface in layers or lifted in clouds (Worms et al. 2000; Hadamcik et al. 2002; current instruments are described in Section 2). Very absorbing materials were studied, C-black, coals and graphite were lifted in an optical thin cloud to measure the single scattering of the particles; the same samples (material and size distribution) were also deposited in sifted or packed layers; their albedo was estimated to a range between 0.002 and 0.1. The PPCs of the three samples composed by carbon particles are presented in Fig. 3. Table 2 gives the main parameters of the PPC. The comparison of $P_{max}$ between lifted and deposited particles with similar sizes indicate that single scattering also dominates the polarization for dark deposited particles. For C-black, $P_{max}$ decreases from about 85 % to about 50 % when the size of the constituent grains increases from 14 nm to 95 nm (Fig 2, left) as usually observed for such fluffy aggregates with submicron-sized constituent grains. $P_{max}$ for the lifted samples has about the average values between the two compactions of deposited samples. For large compact coal particles (100 µm-sized), $P_{max}$ for deposited layers is slightly higher (+15%) than for lifted particles and $\alpha_{max}$ is shifted by +10° for deposited layers (Fig 2, center). For the Huge Deposited (HD) agglomerate (Fig. 2, right) with graphite micrometre-sized constituent grains and for tens to hundred micrometres small lifted (SL) agglomerates, $P_{max}$ has also about the same value around 55 % and $\alpha_{max}$ is shifted by +10° for the HD agglomerate (Hadamcik et al., 2007b). The high porosity HD agglomerate has about 2 cm diameter and 0.5-1 cm height for the light scattering studies and was produced by random ballistic deposition (Blum & Schräpler 2004).

The shift to larger values in phase angle $\alpha_{max}$, between lifted and deposited particles, was systematically observed during the experiment, while its amplitude depends on the albedo (related to size and porosity). For absorbing materials, it ranges from a few degrees up to 30-40°. It can be larger for large transparent particles, up to 60° between 90° ± 10° for lifted particles to 150° ± 20° for deposited ones e.g. for large quartz particles (Levasseur-Regourd et al. 2015).

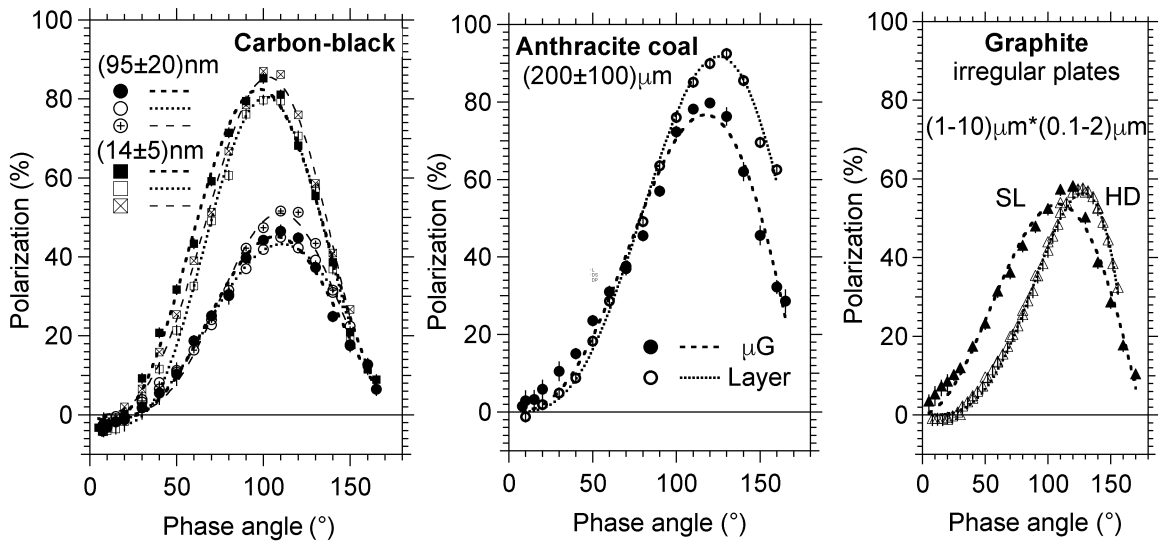


**Figure 2.** PPC for samples made of carbon material with different sizes for the constituent grains. Left: C-black in fluffy aggregates with constituent grains in the tens nanometres size ranges (full symbols for lifted particles, open symbols for deposited sifted particles, symbols with cross for deposited packed particles). Center: Anthracite coal in compact particles (lifted particles, layer for deposited particles). Right: graphite in agglomerates. HD=huge deposited agglomerate, LS= lifted small agglomerates). SEM images of the particles can be found in Hadamcik et al. (2002; 2006; 2007b).

**Table 2**. Three examples with carbon particles lifted in microgravity or deposited in layers. For each material: sizes of the constituent grains and particles (compact or agglomerated), HD = Huge Deposited agglomerates, LS = Small Lifted agglomerates, $P_{max}$ and $\alpha_{max}$ for the 2 configurations. PPCs presented on Fig. 3.

| Materials | Sizes grains/particles | $P_{max}$ (%) Deposited Sifted/packed | $\alpha_{max}$ (°) Deposited Sifted/packed | $P_{max}$ (%) Lifted | $\alpha_{max}$(°) Lifted |
|---|---|---|---|---|---|
| Carbon-black | 14 nm / ≈100 μm<br>95 nm / ≈75 μm | 80.5±0.1/85.5±0.1<br>43.2±0.3/51.4±0.3 | 101.5±0.5/100.0±0.5<br>110.7±0.2/109.3±0.5 | 82.5 ± 0.2<br>45.1 ± 0.5 | 97.5 ± 02<br>106.6 ± 0.2 |
| Anthracite | 200 μm ± 100 μm | 91.7 ± 1.0 | 126 ± 2 | 76.7± 3 | 117 ± 2 |
| Graphite | $(1-10)*(0.1-2)$ μm / D ≈ 2 cm SL ≈ 60 μm | 57 ± 2 | 128 ± 2 | 53 ± 3 | 118 ± 2 |

A summary of the polarimetric properties as a function of the sizes is given below:

(i) $P_{max}$ have similar values for lifted and deposited particles made of carbon grains smaller than 0.2 μm in fluffy aggregates and for hundreds of μm-sized grains e.g. in coals.

(ii) $P_{max}$ have similar values for transparent or absorbing sub-micron sized grains which can be included in aggregates. Larger grains than about 10 μm of transparent materials present a $P_{max}$ value lower than 40 % that decreases to values lower than 10 % for grains in the 100 μm range when lifted and 2 μm range when deposited (multiple scattering). Finally, for larger transparent grains, $P_{max}$ increases again up to about 20 % for large grains of 300 μm range or more (Hadamcik et al. 2009a).

(iii) More generally, when the size of constituent grains in aggregates (or the size of compact particles) increases from 0.01 μm to 0.2 μm, $P_{max}$ decreases. On the opposite, when constituent grains larger than the wavelength increases, $P_{max}$ increases.

(iv) A saturation of the $P_{max}$ values as a function of the absorbing particles size appears for large particles. $P_{max}$ remains constant when the incident light entering the particle is about completely absorbed**.** In that case, the scattered light is only due to reflexion on the surface and the scattering by its irregularities and/or by small grains on the surface, and produces multiple scattering between the particles**.** A systemat**ic** shift of $\boldsymbol{\alpha_{max}}$ to higher values is also observable when $P_{max}$ increases with the size for transparent or absorbing particles (Shkuratov & Openasenko 1992). In conclusion, for absorbing materials $P_{max}$ seems to depend mainly on single scattering by the particles for all the configurations and $\alpha_{max}$ depends on multiple scattering between the particles at the surface layer.

For submicron-sized grains in fluffy aggregates when lifted, $P_{max}$ decreases as the size of the grains increase up to 0.2 μm, with a minimum value of about 40 % for amorphous carbon. For larger sizes, $P_{max}$ increases up to about 80-90 % for carbon. For deposited particles, a similar trend is observed for absorbing carbon materials (Hadamcik et al. 2009a). It is interesting to note that $P_{max}$ may have the same high values (more than 50%), for submicron and hundred μm-sized large dark grains (or particles) and similar values may be observed for deposited and lifted particles.

PROGRA2 current instruments to study light scattering by particles are described in Section 2. In Section 3, dark meteorites (Orgueil and Allende) are suggested as analogues, and the samples size distributions in the three experimental configurations are presented together with their phase curves. Finally, $P_{max}$ variations as a function of the size of the particles is presented allowing to conclude that mm-sized particles must be present on the asteroids surface. Section 4 is a discussion suggesting different materials on the surface of the particles. Conclusions and perspectives are in Section 5

## 2 PROGRA2 INSTRUMENTS AND METHODS

In PROGRA2 previous measurements, photodiodes were used as detectors instead of cameras. To limit the contribution of noise in the signal, only the brightest radiance was taken into account to calculate the polarization (Worms et al. 1999). After the implementation of cameras and using the lifted brightest particles on the images, the agreement with previous results was verified. Thus, the previous measurements (on clouds or surfaces) on carbonaceous chondrites (Worms et al., 2000; Hadamcik et al., 2011) are reassessed using specifically the imaging technique and more sensitive cameras on the experiments.

New versions of the laboratory PROGRA2 experiment and its instruments are dedicated to

measure, by an imaging technique, the brightness and linear polarization of the light scattered by dust particles as a function of the phase angle (Renard et al. 2002; 2014; Hadamcik et al. 2009b; Levasseur-Regourd et al. 2015). To simulate regoliths, the particles are deposited in layers on a horizontal surface in the laboratory. To simulate clouds of solid particles such as those found in cometary comae, ejected by active asteroids, solid aerosols in the atmospheres of planets, the particles are lifted either by an air-draught (in the laboratory) or in micro-gravity conditions (at 0 ± 0.05 g) during dedicated parabolic flights campaigns in an airplane. Particles, that are smaller than 20 μm or than 50 μm whenever they present a very high porosity, may be studied by the air-draught technique. The size of the particles (eventually agglomerates) is ranging from twenty to hundred-μm. The light sources are unpolarised and the measurements in the visible can be conducted at 540 nm and 630 nm.

The size distribution of the original (generally individual) particles is measured using Scanning Electron Microscope images (SEM), or eventually a size range is defined by sieving the samples and separating them from the fine dust. When lifted, the particles may remain well separated (called hereafter 'original particles') or may form agglomerates. They freely float with random movements in a vial during the 22s of a parabola during the microgravity flights, or during several seconds when particles are lifted by air-draught. The images with only a small number of particles are kept to avoid multiple scattering between the particles and to have an optically thin medium. Several tens of images are necessary to retrieve the mean scattering properties of the particles at a given phase angle (with details on data processing within Hadamcik et al. (2009b). The intensity I and the polarization P are computed for each pixel of the polarized images to retrieve intensity and polarization maps. Polarimetric phase curves are built for the whole cloud of particles detected on the polarization maps. The intensity is normalized using a third camera at a fixed phase angle of 90°.
The size distribution of the particles in the field of view is measured on the polarization maps. Fig. 3 presents typical intensity and polarization images for Orgueil meteorite at a phase angle of 90° for particles lifted under micro-gravity conditions. Two large particles (in the 200-600 μm range) are visible, together with smaller ones. The particles, which may be original particles or their agglomerates present irregular shapes. The values are colour- coded for better visibility.
The equivalent diameter of the particles (in pixels) is given by equ.4.

$$d = \sqrt{\frac{4S}{\pi}} \qquad (4)$$

S is the projected surface. The averaged polarization, for a size range of particles on the polarization maps, is deduced by using successive images and averaging the results. To detect a statistically significant mean polarization value as a function of the size of the particles, P needs to be measured for at least several tens of particles for each size range (Renard et al. 2021).
The particles are mostly not mono-dispersed; they present a size distribution which may be log-normal or a power law. For lifted particles, using the polarization maps, the experiment allows to study polarization values for size differences in the 50 μm intervals from about 20 μm to hundreds of μm in microgravity conditions and to about 200 μm with the air-draught technique.

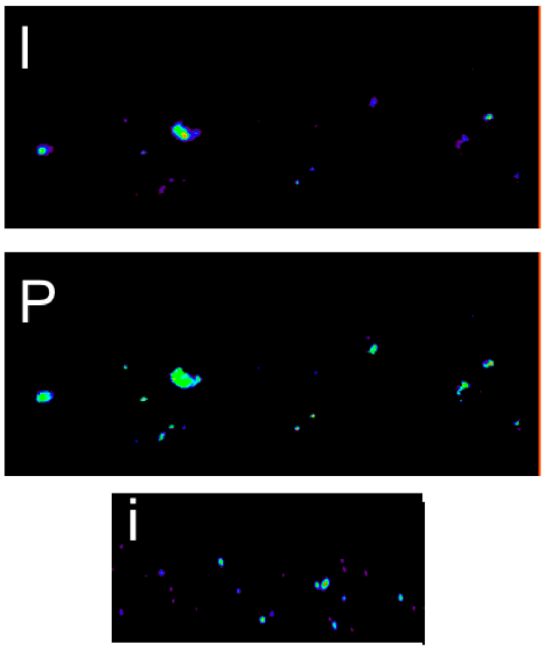


**Figure 3.** Orgueil meteorite particles lifted in microgravity conditions. Phase angle 90°, Field of view 8 mm x 3.4 mm, Intensity 'I' (up), Polarization 'P' (middle), Reference intensity 'i' map at a fixed phase angle, allowing normalization of the intensity (down). Intensity images are in arbitrary units with red for high intensities and purple for low intensities. The polarization maps are in percent, red is for 100 % polarization and purple for -50 %.

Experimental results are presented in the next section. The purpose is to interpret the large polarimetric values obtained for low-albedo

asteroids at large phase angles in terms of physical properties of the particles on their surface. To study experimentally the regoliths of such asteroids, layers of deposited particles with different size distributions were conducted in Earth gravity, including sifted samples. This method allows a first estimation but the obtained porosities of the layers are relatively small as compared to low gravity asteroids. However, particles that are lifted in the experiment can present very high porosities in large agglomerates.

## 3. ANALOGUES FOR DARK ASTEROIDS

It is logical to suggest carbonaceous chondrites as analogues for low-albedo asteroids. Licandro et al. (2007) and Lauretta et al. (2019) suggested for Phaethon and for Bennu CV or CM-types meteorites. For Ryugu, Grott et al. (2020), suggest CI or heated CM chondrites. Yada et al. (2022) discussed the absence of sub-mm Ca-Al-rich and chondrules inclusions in particles above mm sizes, suggesting similarities with CI chondrites but with a lower albedo and higher porosity. The granular material forming the regolith is considered to result from hyper-velocity impacts that pulverize the rocky materials, the smaller-sized particles falling back and forming progressively the regolith layers. In the case of small asteroids, the gravity decreases as compared to large objects, and the smaller-sized particles may be lost either by ejection or by charging processes.

Powdered samples of meteorites Orgueil (CI1-type) and Allende (CV3-type), have been used with different size distributions either deposited on surfaces (sifted or packed), lifted in a vial by an air-draught or even under micro-gravity conditions, to measure the linear polarization of the scattered light (eventually in large high porosity agglomerates) and to compare it with previous observations. The deposited particles are studied under the Earth gravity, although it does not exactly reproduce the low gravity conditions on the surface of a small asteroid. Nevertheless, it was shown in Section 1.3.2 that an estimation of the maximum polarization can be obtained for dark materials by studying the same samples lifted and/or deposited on a surface. Thus, in the following studies, configurations with deposited and lifted particles will be used together, mainly at maximum of the PPC which is extremely sensitive to the size and porosity of the particles.

### 3.1 Samples

For both Orgueil and Allende samples, the carbonaceous material is mainly in the form of organic aromatic matter (Bonal et al. 2006; Remusat et al. 2019). Orgueil meteorite is dark brown with a geometric albedo about 0.05-0.06, (Zellner et al. 1977); and is mainly composed of agglomerated micron-sized grains with a porosity of about 30 %. The particles present irregular shapes after they having been crushed and sieved (Fig 4). Allende meteorite is brown-grey, with a geometric albedo about 0.1. It contains chondrules, which are mainly composed of olivine crystals. Olivine is also a constituent within the matrix. In the powdered sample, some flat surfaces are visible with sharp edges. Numerous small slabs are also detected together with more rounded shapes (Fig. 4). The porosity of the grains is about 23 ± 5 % (Consolmagno, Britt & Macke 2008). They have experienced aqueous alteration and thermal metamorphism (Bonal et al. 2006) which may induce changes in the polarization values whenever NEAs are close to the Sun. Hydrated minerals are decomposed and dehydrated by heating (Ohtsuka et al. 2009).
Different size ranges have been prepared with particles smaller than 500 μm for measurements during parabolic flights and smaller than 50 μm for the air-draught technique. The size distributions of the particles on SEM images (original particles) and the size distributions measured on the polarization maps for the two meteorites are presented on Figs.5a & 5b.

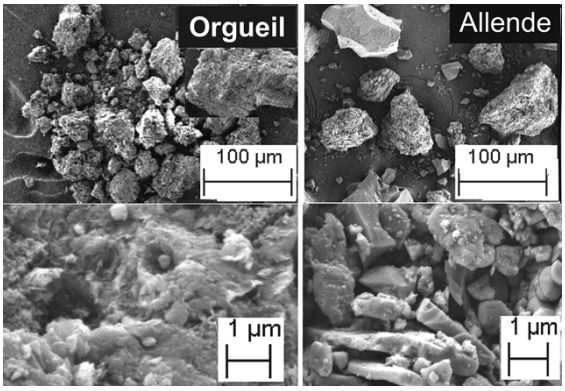


**Figure 4.** SEM images of Orgueil and Allende meteorites showing their structure.

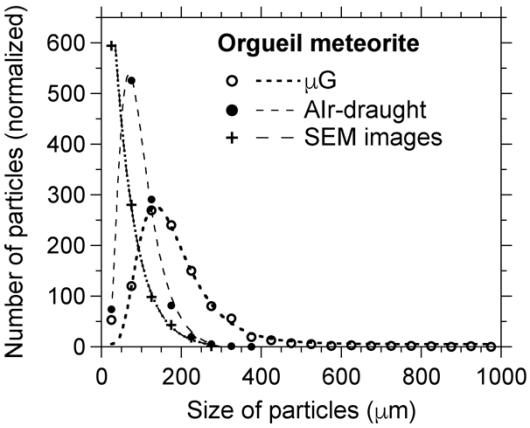


**Figure 5a:** Size distributions for Orgueil meteorite from SEM images and polarization maps. The number of particles is normalized to a total of 1000. The fits are Log-normal laws. All the original particles are smaller than 600 µm on the SEM images.

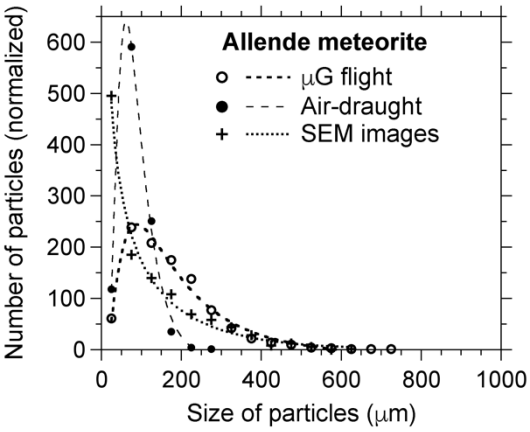


**Figure 5b:** Same than Fig. 5a, for Allende

For each size range, larger than about 100 µm the number of lifted particles is higher than the number of original particles showing the presence of agglomerates (Fig. 5a and 5b). Larger particles are detected, up to 1000 µm for Orgueil and 700 µm for Allende for micro-gravity conditions and up to 400 µm and 300 µm for the air-draught conditions (Fig. 5a and 5b). Particles of some hundreds of micrometres may appear as single particles on the polarization maps of the instrument. The 'original' particles that were at the bottom of the vial before the levitation are agglomerated by contact with each other, making large particles when they are lifted (Van der Waals forces between the original particles and eventually electrostatic forces allowing small grains to stick together or on larger ones, forming large agglomerates).

### 3.2 Phase curves

For the two meteorites, PPCs are built for the three configurations air-draught and micro-gravity in Fig. 6a and deposited layers in Earth gravity in Fig. 6b. Trigonometric fits are applied to retrieve the main parameters of the PPCs (Penttilä et al. 2005), they are listed in Table 3.

For lifted Orgueil meteorite, $P_{max}$ increases from about 26.3 % (air-draught) up to 36.3 % (micro-g) at $\alpha_{max}$ about 90°. For lifted Allende meteorite, $P_{max}$ increases from 13.4% at $\alpha_{max}$ about 105° (air-draught) to 21.4% (micro-g) at $\alpha_{max}$ about 115° when the size of the particles increases. The smaller values of $P_{max}$ for Allende may correspond to its slightly higher albedo. $\alpha_{max}$ is shifted toward higher values by 10-12°.

Only one PPC is available for Orgueil in the largest size distribution for deposited samples with $P_{max}$ = 20.5 % at $\alpha_{max}$ = 100°. For the smaller sizes only a $P_{max}$ = 13 % at 95° can be measured. To have a best precision on the variation of $P_{max}$ as a function of size, measurements were conducted just close to the maximum polarization for four narrower (±20 µm) values of the sizes around 100 µm, 150 µm, 200 µm and 300 µm (Fig. 7a). For Allende deposited on a surface, $P_{max}$ = 25.8 % at 120° for the largest sizes and $P_{max}$ = 17.7 % at 110° for the smallest size distribution

.

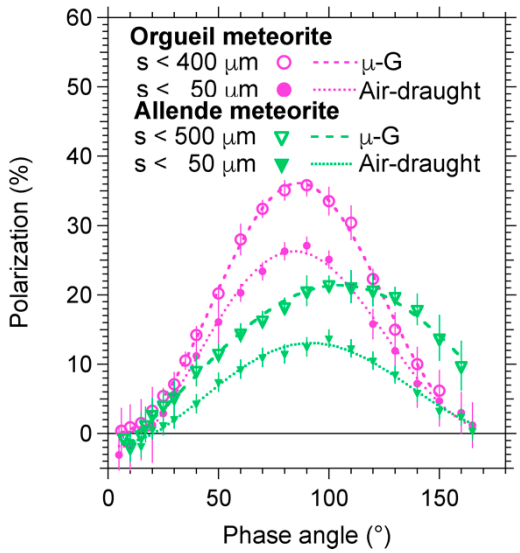


**Figure 6a.** PPCs for the 2 meteorites lifted by air-draught and in micro-gravity conditions. Red wavelength domain.

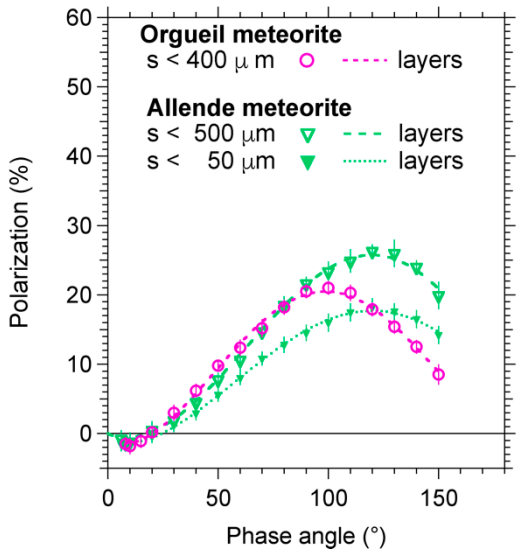


**Figure 6b.** PPCs for the 2 meteorites sifted on a plane surface. Red wavelength domain.

For Orgueil, $P_{max}$ is higher for lifted particles than for layers, this result can be due to the numerous very large levitating agglomerates in the field of view (Fig. 6a & 6b). For Allende, $P_{max}$ is higher for deposited layers than for lifted particles, larger particles being eventually present on the surface of the sample (Brazil nut effect, Rosato et al. (1987)).

The maximum polarization for all of these samples never reaches values of the order of 50 %. This result may be due to a smaller average size of the particles as compared to those found at the surface of the asteroids. Also, the systematic shift of $\alpha_{max}$ for Allende as compared to Orgueil may also be due to some multiple scattering effect corresponding to the higher albedo for Allende. Other parameters may be invoked, such as the microporosity of the particles.

### 3.3 $P_{max}$ and size of the particles

Figures 7a and 7b present the variation of the maximum polarization as a function of the size of the particles for the two meteorites in the three configurations (deposited in layers, lifted by air-draught or during micro-gravity conditions). As for deposited particles, $P_{max}$ increases up to a maximum value when all the incident light is completely absorbed by the material (except the scattered light by the external surface of the particles). Since the particles are dark and their surface is mainly rough, multiple scattering between the original particles inside the agglomerates is limited mainly for Orgueil. The asymptote of an exponential fit applied to the data allows to estimate the maximum polarization which would be obtained for each sample and configuration. The function used to fit $P_{max}$ is given by relation (5), where x is the size of the particles.

$$Fit_P_{max} = Coeff1+Coeff2*exp(-coeff3*x) \quad (5)$$

The different coefficients and their error bars calculated for each fit are given for the two meteorites in Table 4. Coeff1 is the asymptote value extrapolated on the curve and indicate the higher $P_{max}$ which may be obtained from these fits. Values for $P_{max}$ are calculated for particles of 1 mm and 3 mm which cannot be measured directly by the experiment; the difference between the results at 3 and 1 mm being close to the error bars on the coefficients; moreover, for 3 mm-sized particles in the 3 configurations, $P_{max}$ has about the asymptote value (coeff1).

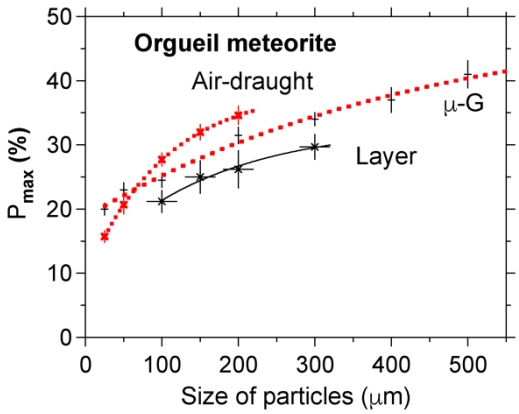


**Figure 7a.** Orgueil meteorite: $P_{max}$ vs size of the particles in the 3 configurations; for deposited particles the size is measured using sieves; for lifted particles, the equivalent size is deduced from the polarization maps.

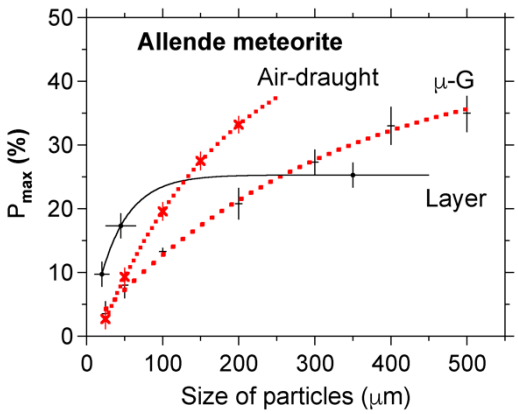


**Figure 7b**. Allende meteorite. Same than for Orgueil

Some conclusions can be derived:
For meteorite, in the three configurations, $P_{max}$ increases similarly with the increase of size e.g. between 150 and 200 μm, the slope of increase is (0.050 ± 0.002) % $\mu m^{-1}$.

For both meteorites, $P_{max}$ for lifted particles by air-draught is greater than $P_{max}$ for lifted particles in μ-gravity for all the sizes (greater than 50 μm)

A possible interpretation considering the size distribution of the original particles in the two cases is that the original constituent grains for lifted particles by air-draught are in average smaller than 20 μm. The maximum size of the agglomerates which can be observed with this configuration is about 200 μm; thus, in the agglomerates lifted by air-draught, the constituent particles have a relatively small size distribution. In microgravity the size distribution for lifted particles is more extended (20-500 μm). For a given agglomerate size, the microporosity of the agglomerates would be higher in micro-gravity than when the particles are lifted by an air-draught from the ground, due to the larger polydispersion of the particles (Grott et al. 2020), thus giving lower polarization.

Taking into account all the uncertainties presented above, we can conclude that when the fits are extrapolated up to mm-sized large particles, the polarization may be close to 40-50 % for all the lifted particles for the two carbonaceous chondrites (Table 4). For deposited particles in Earth gravity, $P_{max}$ is smaller than when the particles are lifted in large agglomerates.
Nevertheless, It was shown previously that for dark particles, $P_{max}$ has about the same value or is slightly higher for deposited particles in a layer than for lifted ones. This suggests that for regoliths in loose layers of dark particles in a mm-sized range or more, the polarization at maximum would be about 50 % or slightly more, depending on the porosity of the particles and of the layer. The phase angle at maximum is shifted to higher values for the deposited layers (e.g. shift 10° for Orgueil and 20° for Allende).

**Table 3.** PPCs parameters for Orgueil and Allende meteorites measured in Earth gravity. Red Domain.

| | $\alpha_{min}$ (°) | $P_{min}$ (%) | $\alpha_0$ (°) | h (%/°) | $\alpha_{max}$ (°) | $P_{max}$ (%) |
|---|---|---|---|---|---|---|
| **Orgueil** | | | | | | |
| μ-G (<400 μm) | -- | -- | 18 ± 2 | 0.58 ± 0.02 | 89.3 ± 1 | 36.3 ± 0.1 |
| Air-draught (<50 μm) | 8 ± 2 | -1.8 ± 0.5 | 17.1 ± 1.1 | 0.34 ± 0.02 | 86.5 ± 1 | 26.3 ± 0.1 |
| Layer | | | | | | |
| <400 μm | 8 ± 2 | -1.4 ± 0.4 | 20.0 ± 1.0 | 0.20 ± 0.02 | 100 ± 3 | 20.5 ± 0.5 |
| <50 μm | -- | -- | -- | -- | 95 ± 5 | 13 ± 2 |
| **Allende** μG | | | | | | |
| <500 μm | 8.5 ± 2.0 | -0.9 ± 0.4 | 15 ± 2 | 0.25 ± 0.02 | 105 ± 2 | 21.4 ± 0.1 |
| Air-draught <50 μm | 10 ± 2 | -1.2 ± 0.5 | 20 ± 3 | 0.17 ± 0.02 | 98 ± 2 | 13.4 ± 0.4 |
| Layer | | | | | | |
| <500 μm | 8.3 ± 2.3 | -0.5 ± 0.3 | 17.3 ± 1.2 | 0.11 ± 0.01 | 120 ± 3 | 25.8 ± 0.5 |
| <50 μm | 8.2 ± 2.0 | -1.4 ± 0.6 | 18.0 ± 1.3 | 0.16 ± 0.01 | 110 ± 4 | 17.7 ± 0.6 |

**Table 4**. Exponential fit. In the two last columns $P_{max}$ for 1mm and 3 mm sized particles.

| | Coeff1 | Coeff2 | Coeff3 | $P_{max}$ (%) for D=1 mm (%) | $P_{max}$ (%) for D=3mm |
|---|---|---|---|---|---|
| **Orgueil** | | | | | |
| Deposited layer | 33.0 ± 2.5 | -21.5 ± 2.2 | 0.00616±0.00261 | 32.4 ± 2.5 | 33.0 ± 2.5 |
| Lifted by air-draught | 38.74 ± 0.03 | 29.46 ± 0.02 | 0.00982±0.00426 | 38.73 ± 0.01 | 38.7 ± 0.4 |
| Lifted in μG | 50.8 ± 5.0 | 32.0 ± 4.6 | 0.00225±0.00065 | 45 ± 3 | 51 ± 5 |
| **Allende** | | | | | |
| Deposited layer | 25.3 ± 0.2 | 2.6 ± 0.1 | -0.0267±0.0052 | 25 ± 1 | 25 ± 1 |
| Lifted by air-draught | 50 ± 1 | 54.75 ± 0.6 | -0.0059 ± 0.0006 | 50 ± 1 | 50 ± 1 |
| Lifted in μG | 44.8 ± 2.6 | 43.9 ± 2.2 | 0.00313±0.00041 | 43 ± 2 | 45 ± 3 |

## 4. DISCUSSION

To reach the high polarization of about 50 %, observed for low-albedo asteroids, particle sizes of a mm-range at the asteroids surface is suggested by the experiment when using the carbonaceous chondrites (Orgueil and Allende) as analogues. Since the five asteroids are dark. It is also possible to consider other materials to obtain such high polarization.

### 4.1 Carbon materials on the surface

Figure 8 presents $P_{max}$ as a function of the size of lifted particles for carbon blacks and coals (the lignite is less dark than the anthracite).
The 50 % polarization is obtained for particles smaller than 100 µm for all the materials. Kuroda et al. (2018) suggested that small nm-sized carbonaceous grains in fluffy µm-sized aggregates can be present on the surface layer of 1998 KU2. Nevertheless, these absorbing materials would produce too small an albedo if they cover the asteroid. They can eventually exist on restricted areas (see also subsection 4.3 for heated regions by the Sun proximity).

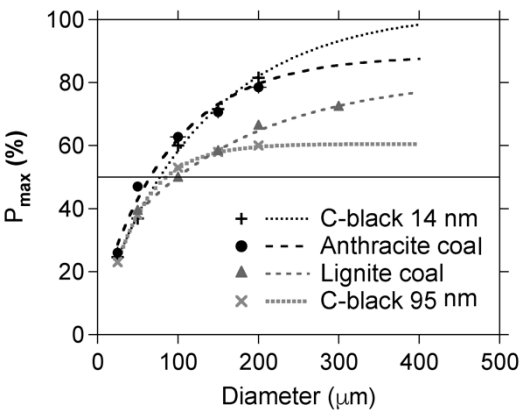


**Figure 8**. $P_{max}$ vs size of the lifted particles. C-blacks are fluffy aggregates; coals (anthracite and lignite) are solid porous particles. Horizontal line is for 50 % polarization.

### 4.2 Mixture of carbon and silicates

Another possibility could be to consider mixed 50 % in mass of C-black with 25 % Mg-silica (transparent) and 25 % Fe-silica (dark grey) as for some cometary particles analogues (Hadamcik et al. 2007a). All the constituent grains of the aggregates are in the [14-50] nm range. The particles are fluffy aggregates in a size range [20-200] µm. A crude estimation of the albedo is 0.06 ± 0.03 for a small quantity of deposited sample. $P_{max}$ in red light was found to be (57 ± 2) %.

### 4.3 Carbonization of surface materials (NEA objects)

All the asteroids considered within this study are NEAs objects, with a small equivalent size (between 0.5 and 6 km). Their perihelion distance is smaller than about 1 au and even below 0.16 au for two of them (Phaethon and 2005 UD). These small solar distances suggest high temperatures at their surface during their close approach to the Sun, which may affect the regolith properties (Ohtsuka et al. 2009, Wittmann et al., 2011). Carbonization is the result of dehydration and more generally loss of volatiles with a decrease of the H/C ratio and also eventually of the N/C ratio. The optical properties change with an increasing absorption of the materials in favour of higher polarizations. Moreover, near the Sun, the objects are not only submitted to solar heating but also to space weathering with enhanced micrometeoritic bombardment and irradiation, indeed expected to be much more efficient closer to the Sun (Marchi et al. 2009). Irradiation of complex hydrocarbons leads to carbonization and changes of their surface layers (Moroz et al. 2004, 2005). As an example, a poly-HCN brown fluffy aggregate lifted sample, heated from ambient temperature to 300°C, initially presented a $P_{max}$ about 45% as opposed to about 75 % after heating (Hadamcik et al. 2010).
Depending on the period of observations, the differences in PPCs for Phaethon, with its highly tilted polar axis, suggest different properties for the illuminated terrains. In consequence, the higher polarization noticed during 2016 observations suggests more materials metamorphosed by heating, probably in the North pole region (Ohtsuka et al. 2009). At the opposite, the observations obtained in December 2017 with a 10 % lower polarization, correspond probably to regions at lower latitudes (Shinnaka et al. 2018). Simulations of heating suffered by meteoritic material on the surface of Phaethon indicate that temperatures in excess of 600°C can be reached for the upper 10 cm of the surface of Phaethon in its current orbit, which would have a significant effect on its material properties and composition (Wittmann et al. 2011).

### 4.4 Particles with very high porosities

Space missions to Ryugu and Bennu confirm their very small bulk-density (respectively 1.27 and 1.26) and in consequence the presence of particulates regolith (DellaGiustina et al. 2019; Sakatani et al. 2021). Previous measurements, as heat conductivity, thermal inertia and thermal

stress, have suggested the presence of cm-sized particles in regoliths (Gundlach & Blum 2013; Delbo et al. 2014). The first results of Hayabusa2 mission have given remarkable information on the surface of Ryugu, covered by numerous boulders with porosities between ≈30% and 50 % (e.g. Grott et al. 2019; Okada et al. 2020). Boulders with ultra-high porosities (70 %) were also discovered (Sakatani et al., 2021), and they seem to be consistent with a primitive material, The PPC obtained by remote observations by Kuroda et al. (2021) allows to estimate $P_{max} \geq 53\%$ at $\alpha_{max} \approx 102°$. This value is in the range of the extrapolated $P_{max}$ for Orgueil particles lifted in microgravity with an average size range of 3 mm.

Huge deposited agglomerates with micron-sized black graphite grains are somehow experimental 'boulders'. Their maximum polarization is (57 ± 2) % at a phase angle of 128° (Fig. 3, right, HD curve). One can imagine to consider as analogues huge deposited agglomerates of cm-sizes, made of dark (organic) materials or materials such as carbonaceous chondrites. Huge deposited agglomerates were indeed produced with mixtures of 90 % of graphite plates with a size range of the grains of (1-10) µm * (0.1-2) µm and of 10 % of irregular transparent silica with a size range of [0.1-6] µm. The agglomerate colour is dark grey. Their PPC curves exhibits a $P_{max}$ value of (45 ± 10) % for $\alpha_{max}$ = (120 ± 10)°. The mm- or slightly larger size range of the regolith particles are confirmed by the analysis of the samples already obtained from Ryugu (Yada et al., 2022) where the presence of CI chondrites is also suggested. Nevertheless, the surface reflectivity is smaller for the remote observations than for the recovered materials, which could justify the choice of dark powdered materials at the surface as is proposed in the present paper.

## 5. SUMMARY, CONCLUSIONS AND PROSPECTIVE

Experimental results about the polarized light scattered by dust particles have been compared to observations derived from remote telescopic data and space missions for 5 low-albedo asteroids, Ryugu, 1998 KU2, Bennu, 2005 UD, as well as for Phaethon. The high polarization values at large phase angles are close to 50 % at maximum for four of them. As explained in section 1.2, $P_{max}$ for Bennu, is unknown, a comparison to Ryugu and Phaethon asteroids at intermediate phase angles may suggest a value in the 40-50% range. All have an average diameter smaller than 6 km, leading to a low gravity. Highly porous boulders were indeed observed on two of them (Ryugu and Bennu).

Measurements have been conducted with the laboratory PROGRA2 light scattering experiment with dark particles of Orgueil and Allende meteorites deposited on layers or lifted in clouds. For these low-albedo particles, multiple scattering is negligible and the polarization is governed by single scattering. The polarization at maximum presents comparable values for clouds and layers. The light impacting the particles is mainly absorbed, except from their external surfaces and the phase angle value at polarization maximum is shifted towards higher values for agglomerates and for deposited particles. For lifted particles (which may be agglomerates), the experiment allows us to measure the polarization as a function of particles' sizes. Considering extrapolation up to mm-sized particles, the laboratory measurement can reproduce the 40-50 % polarization measured for these asteroids.

Huge deposited agglomerates (cm-sized) of very high porosity made by absorbing particles (µm-sized) are obtained by random ballistic deposition. They are mechanically stable due mainly to van der Waals forces and can represent fair analogues for pebbles and boulders observed on Ryugu or Bennu. The asteroid regolith could partially result from boulders' breaking. The laboratory maximum polarization of the scattered light by such boulders may also have values as high as 50 %.

Similarities and differences on the PPCs of the five asteroids can be noticed. Ryugu and 1998 KU2 present similar light scattering properties and probable similar physical properties of their surface materials. Ryugu and Bennu PPCs on the positive branch are similar up to a phase angle of 30°. However, the polarization values seem to be slightly smaller for Bennu than for Ryugu at larger phase angles, possibly suggesting smaller sizes for the particles of Bennu. Since Bennu's spectral type is F while Ryugu's is B, differences in composition may also explain a difference in polarization. Finally, Phaethon PPCs may suggest that thermal and space weathered materials at the vicinity of the North Pole produce higher polarization, and the increase of $P_{max}$ being the result of carbonization.

Further information on the physical and chemical properties of the regolith present on these objects is expected from the analyses of samples returned to Earth by Hayabusa2 and OSIRIS-REx. First results from the touch-down sites for Ryugu suggest that mm-size range CI chondrites particles used with PROGRA2 could be good analogues. Finally, the observations of

the surface of Phaethon by Destiny+ during its close flyby will allow to interpret the compositional variations of the surface of Phaethon that was derived from remote polarization observations, which could result from important heating effects of the materials.


## Acknowledgements

F. Pillier (LISE/CNRS/Sorbonne Université) is acknowledged for SEM images analysis. We thank J. Blum and R Schräpler from Institut für Geophysik and Extraterrestrishe Physik/Braunschweig for the random ballistic huge agglomerates. We are grateful to Museum national d'Histoire Naturelle of Paris to have provided the Orgueil meteorite sample and Palais de la Découverte to have provided the Allende meteorite sample. The PROGRA2 microgravity parabolic flights campaigns were funded by the French Space Agency CNES and by the European Space Agency ESA and are operated by Novespace. M.I. was supported by the NRF grant No.2018R1D1A1A09084

ACLR passed away on August 1st, 2022, she initiated this work being always interested by remote observations in complement to space missions and experimental simulations to interpret them. She actively participated to the design of the microgravity PROGRA2 experiment. EH wrote the paper. JBR (PI of PROGRA2) and EH made the experiments, analyzed the results and interpreted them, ACLR and JL contributed in describing the context of the work, and improving the discussion, MI make the link with JAXA and remote observations.


## Data availability

The experimental data underlying this article are available in the PROGRA2 site where the data for numerous samples can be also found: https://www.icare.univ-lille.fr/progra2/

Data used in the different papers may also be obtained from their first authors

## REFERENCES


Arai T. et al., 2018, LPI, 49th Lunar 1Planet Sci,, 2570
Barnouin O.S. et al., 2019, Nature Geosci, 12, 4, 247
Battams K., Knight M.M., Kelley M.S.P., Callagher B.M., Howard R.A., Strenborg G. 2020, ApJS, 246,64
Belskaya I.N. et al., 2017, Icarus, 284, 30.
Blum J. & Schräpler R. 2004, PhysRevL 93, 115503
Bonal L., Quirico E., Bourot-Denise M., Montagnac G., 2006, Geochim Cosmochim A. 70, 1849
Borisov G. et al., 2018, MNRAS, 480, L131
Cellino A., Bagnulo S., Gil-Hutton R., Tanga P., Canada-Assandri M., Tedesco E.F., 2015, MNRAS 451, stv118
Cellino A., Bagnulo S., Christou A., Belskay I. N., 2018, MNRAS, 481, L49
Chesley S.R., 2014, Icarus 235, 5
Consolmagno G.J., Britt D.T., Macke R.J., 2008, Chemie der Erde 68, 1
Delbo M. et al., 2014, Nature, 508, 233
DellaGiustina D. N. et al., 2019, Nature Astronomy, 3, 341
Devogèle M. et al., 2018, MNRAS, 479, 3478
Devogèle M. et al., 2020, Planet. Sci. J. 1:1
Dollfus A. & Bowell E., 1971, A&A 10, 29
Dollfus A., Bowell E. & Titulaer C., 1971, A&A 10, 450
Fornasier S. et al., 2006, A&A 455, 371
Fujiwara A. et al., 2006, Science 312, 13
Geake J.E. & Dollfus, 1986, MNRAS 218, 75
Geem J. et al., 2022, MNRASL1
Grott M. et al., 2019, Nature Astronomy, 3 (11), 971
Grott M. et al., 2020, JGR Planets 125, e2020JE00651
Gundlach B. & Blum J., 2013, Icarus 223, 47
Güttler C. et al., 2019, A&A 630, A24
Hadamcik E., Renard J.-B., Worms J.C., Levasseur-Regourd A.C., 2002, Icarus 155, 497
Hadamcik E., Renard J.-B., Levasseur-Regourd A.C., Lasue J., 2006, JQSRT 100, 143
Hadamcik E., Renard J.-B., Rietmeijer F.J.M., Levasseur-Regourd A.C., Hill H.G.M., Karner J.M., Nuth J.A., 2007a, Icarus 190, 660
Hadamcik E., Renard J.-B., Lasue J., Levasseur-Regourd A.C., Blum J., Schräpler R., 2007b, JQSRT 106
Hadamcik E., Renard J.-B., Levasseur-Regourd A.C., Lasue J., Alcouffe G., Francis M., 2009a, JQSRT 110, 1755
Hadamcik E., Renard J.-B., Levasseur-Regourd A.C., Worms J.C., 2009b, in Khokanovsky AA, editor, Light Scattering Reviews 4, 31
Hadamcik E. et al., 2010, 38th COSPAR Sci. Assembly, abstract E16-002710
Hadamcik E., Levasseur-Regourd A.C., Renard J.-B., Lasue J., Sen A.K., 2011, JQSRT, 112, 1881

Hanus J. et al., 2016, A&A, 620, L8
Ishiguro M., et al., 2021, MNRAS 509, 4128
Ito T. et al., 2018, Nature Com, 2486
Jewitt D., 2012, AJ 143, 66
Kiselev N.N. et al., 2022, MNRAS 514, 4861
Kruger H. et al., 2019, PSS 172, 22
Kuroda D. et al., 2018, A&A 611, A31
Kuroda D. et al., 2021, ApJL 911, L24
*Lauretta D.S. et al., 2015, M&PS 50, 834*
*Lauretta D.S. 2019, Nature, 568, 7750, 5*
Levasseur-Regourd A.C., Hadamcik E., Lasue J., 2006, Adv. Space Res. 437, 161
Levasseur-Regourd A.C., Renard J.-B., Shkuratov Y., Hadamcik E., 2015, in Kolokolova et al. Eds, Polarimetry of stars and planetary systems, Cambridge University Press, p. 62
Licandro J., Campins H., Mothé-Diniz T., Pinilla-Alonso N., de Leon J., 2007, A&A 461, 751
Marchi S., Delbo M., Morbidelli A., Paolicchi P., Lazzarin M., 2009, MNRAS 400, 147
Masiero J.R., Wright E.L., Mainzer A.K., 2019, Astrophys. J 58, 97
Moroz L., Baratta G., Strazzulla G., Starukhina L., Dotto E., Barucci M.A., Arnold G., Distefano E., 2004, Icarus 170, 214
Moroz L., 2005, LPS XXXVI, 2056
Muñoz O. et al., 2020, Astrophys. J.SS 247, 19
Nugent C. R. et al., 2016, AJ 152, 63
Okada T. et al., 2020, Nature 579, 518
Okasaki R. et al., 2020, PSS 180, 104774
Ohtsuka K., Nakato A., Nakamura T., Kinoshita D., Ito T., Yoshikawa M., Hasegawa S., 2009, PASJ 61, 1375
Penttilä A., Lumme K., Hadamcik E., Levasseur-Regourd A.C., 2005, A&A, 432, 1081
Remusat L., Bonnet J.Y., Bernard S., Buch A., Quirico E., 2019, GCA 263, 235
Renard J.-B., Worms J.C., Lemaire T., Hadamcik E., Huret N., 2002, Appl. Opt. 41, 609
Renard J.-B., Hadamcik E., Couté B., Jeannot M., Levasseur-Regourd A.C., 2014, JQSRT, 146, 424
Renard J.-B., Geffrin J.-M., Tobon Valencia V., Tortel H., Ménard F., Rannou P., Milli J., Berthet G., 2021, JQSRT 272, 107718
Rosato A., Strandburg J., Prinz F., Swendsen R.H., 1987, Phys RevL 58, 1038
Sakatani N. et al., 2021, Nature Astronomy, 5,766
Shinnaka Y., Kasuga T., Furusho R., Boice D.C., Terai T., Noda H., Namiki N., Watanabe J-I., 2018, AJL, 864, L33
Shkuratov Yu. G.& Opanasenko N.V., 1992, Icarus 99, 468,
Shkuratov Yu. G., Bondarenko S., Ovcharenko A., Pieters C., Hiroi T., Volten H., Muñoz O., Videen G., 2006, JQSRT 100, 340
Shkuratov Yu, G., Bondarenko S., Kaydash V., Videen G., Muñoz O., Volten H., 2007, JQSRT 106, 487
Shkuratov Yu., G., Kaydash V., Korokhin V., Velikodsky Y., Opanasenko N., Videen G., 2011, PSS 59, 1326.
Sugita S. et al., 2019, Science 364,252
Umov N.A., 1905, Phis. Zeits 6, 674
Volten H., Muñoz O., Hovenier J.W., Rietmeijer F.J.M., Nuth J.A., Water B.F.M, van der Zande W.J., 2007, A&A 470, 377
Walsh K.J. et al., 2019, Nature GeoScience 12, 242
Watanabe S. et al., 2017, Space Sci. Rev, 208, 3
Watanabe S. et al., 2019, Science 364, 268
Wittmann A. et al., 2011, GCA 75, 6140
Worms J.C., Renard J.-B., Hadamcik E., Levasseur-Regourd A.C., Gayet J.-F., 1999, Icarus 142, 281
Worms J.C., Renard J.-B., Hadamcik E., Brun-Huret N., Levasseur-Regourd A.C., 2000, PSS 48, 493
Yada T. et al., 2022, Nature Astronomy Letters, vol 6, 214
Yoshikawa M., Kawaguchi J., Yano H., 2010, 41st Lunar and Planetary Science Conference, LPI, 2746
Zellner B., Leake M., Lebertre T., Duseaux M., Dollfus A., 1977, LPSC VIII, 1091
Zheltobryukhov M., Chornaya E., Kpchergin A., Kornieneko G., Matkin A., Ivanova O., Luk'yanyk I., Zubko E., 2018, A&A 620, A179
Zubko E., Videen G., Shkuratov Y., Muinonen K., Yamamoto T., 2011, Icarus 212, 403
Zubko E., Videen G., Hines D.C., Shkuratov Y, 2016, PSS 123, 63